EurJIC European Journal of Inorganic Chemistry

ChemPubSoc Europe

FULL PAPER

DOI:10.1002/ejic.201201378

Experimental and Computational Investigations of Tautomerism and Fluxionality in PCP- and PNP-Bridged Heavy Chalcogenides

Philip J. W. Elder,[a] Tristram Chivers,*[a] and Ramalingam Thirumoorthi[a]

Keywords: P ligands / Chalcogens / Tautomerism / Fluxionality / Density functional calculations

The reaction of $H_2C(PCl_2)_2$ with four equivalents of *i*PrMgCl produces $H_2C(PiPr_2)_2$, which was treated with tellurium in boiling toluene, or selenium in toluene at room temperature, to give the monochalcogenides $EPiPr_2CH_2PiPr_2$ (E = Te, **4a**; E = Se, **4b**) in high yields. X-ray structural determinations show that **4a** and **4b** exist as the CH_2 tautomers in the solid state with E–P–C–P dihedral angles of 56.1(2)° and 56.7(1)°, respectively. DFT calculations were carried out for the isolectronic series $EPR_2CH_2PR_2$ and EPR_2NHPR_2 (E = Se, Te; R = Me, *i*Pr, *t*Bu, Ph) and for their non-chalcogenated precursors in order to elucidate the factors that determine the preference for PH tautomers in some PNP-bridged systems. Compounds **4a** and **4b** were also characterized by multinuclear (^1H, ^{13}C, ^{31}P, ^{77}Se, ^{125}Te) NMR spectroscopy. In solution, **4a** exhibits fluxional behavior, which has been investigated by variable-temperature and variable-concentration multinuclear NMR spectroscopy. The observed behavior is consistent with an intermolecular tellurium transfer with an activation energy of 21.9 ± 3.2 kJ mol^{-1}; consideration of selenium exchange in **4b** indicates a much higher energetic barrier. DFT calculations provide insights into the pathway for the chalcogen exchange process in **4a** (ΔE = 20.4 kJ mol^{-1}). The outcome of reactions of **4a** with selenium and *n*BuLi reflects the lability of the P-Te functionality.

Introduction

Extensive studies of the redox chemistry and coordination complexes of tellurium-centered PNP-bridged ligands of the type $[TePR_2NPR_2]^-$ (**1**) and $[N(PR_2Te)_2]^-$ (**2**) (R = *i*Pr, *t*Bu) have been reported recently.[1] In certain cases, metal complexes of **2** serve as suitable single-source precursors for binary metal tellurides in the form of thin films or nanocrystals.[2,3] The synthesis of these tellurium-centered ligands requires a different approach than that employed for the lighter chalcogen analogues because tellurium is a weaker oxidant than sulfur or selenium towards the P^{III} centers in the neutral precursors $HN(PR_2)_2$. For example, when R = Ph, tellurium is inert even in boiling toluene; however, for R = *i*Pr, the monotelluride is obtained in high yield as the PH tautomer $HPiPr_2NP(Te)iPr_2$ (**3a**) upon treatment of $HN(PiPr_2)_2$ with one equivalent of tellurium in *n*-hexane at 23 °C.[4] The selenium analogue **3b** also forms the PH tautomer both in the solid state and in solution.[5] The monotelluride **3a** is readily metallated with *n*BuLi to give **1** (R = *i*Pr), which, although it is unstable towards disproportionation, can be used as an in situ reagent for the synthesis of homoleptic group 11 and 12 complexes.[6]

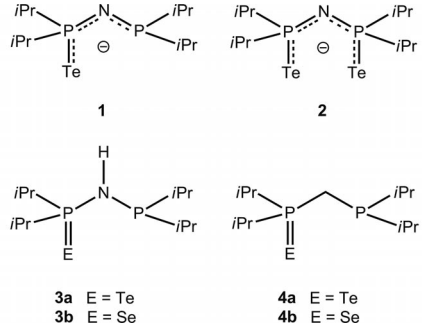

In early work, Lusser and Peringer generated the monotelluro PCP-bridged anion $[TePPh_2C(H)PPh_2]^-$ as the Li derivative by a *metallation-first* approach in which the P^{III}/P^{III} precursor $Ph_2PCH_2PPh_2$ was lithiated with *n*BuLi *prior to* oxidation with tellurium.[7] This in situ reagent was then used to prepare a homoleptic Hg^{II} complex that was characterized only by ^{31}P and ^{199}Hg NMR spectroscopy.[7] In 2009, we obtained an X-ray crystal structure of (TMEDA)-Li[$TePPh_2C(H)PPh_2$], which comprises a centrosymmetric dimer incorporating a weak Te···Te contact [3.514(1) Å].[8] However, this lithium complex is extremely moisture-sensitive and disproportionates readily in solution.[8]

Tellurium-centered PCP-bridged ligands with P-alkyl substituents have not been characterized. In this investigation, we intended to compare the structure, properties, and reactions of the PCP-bridged monochalcogenides

[a] Department of Chemistry, The University of Calgary, Calgary, AB, T2N 1N4, Canada
Fax: +1-403-289-9488
E-mail: chivers@ucalgary.ca
Homepage: www.ucalgary.ca/chem/

EP*i*Pr$_2$CH$_2$P*i*Pr$_2$ (E = Te, **4a**; E = Se, **4b**) with those of the PNP-bridged analogues **3a** and **3b**. In particular, we sought to ascertain whether **4a** and **4b** form the CH_2 tautomer in preference to the PH tautomer. In that context, we report here high-yield syntheses of **4a** and **4b** together with their X-ray crystal structures. In view of this finding, we carried out a comprehensive DFT computational study for the isoelectronic series EPR$_2$CH$_2$PR$_2$ and EPR$_2$NHPR$_2$ (E = Se, Te; R = Me, *i*Pr, *t*Bu, Ph) and for their non-chalcogenated precursors that provides a clarification of the factors, which determine the preference for PH tautomers in some cases. The solution behavior of **4a** and **4b** has been investigated in detail by variable-temperature and, in the case of **4a**, variable-concentration multinuclear (^{1}H, ^{31}P, and ^{125}Te) NMR spectroscopy, which reveals fluxional behavior involving tellurium exchange. DFT calculations have been conducted in order to elucidate the pathway of the tellurium-transfer process. The reactions of **4a** with selenium, tellurium, and *n*BuLi have also been studied with a view to evaluating the influence of the labile P–Te bond on oxidation or deprotonation processes.

Results and Discussion

Synthesis and X-ray Structures of TeP*i*Pr$_2$CH$_2$P*i*Pr$_2$ (4a) and SeP*i*Pr$_2$CH$_2$P*i*Pr$_2$ (4b)

We recently developed a high-yield route to the diseleno PCP-bridged anion [HC(P*i*Pr$_2$Se)$_2$]$^-$ as the Li$^+$ derivative using the commercially available bis(dichlorophosphinoyl)-methane H$_2$C(PCl$_2$)$_2$ in a three-step process.[8] In this work, a similar approach led to the isolation of the monotelluride TeP*i*Pr$_2$CH$_2$P*i*Pr$_2$ (**4a**) as a pale yellow powder in 98% yield and the monoselenide SeP*i*Pr$_2$CH$_2$P*i*Pr$_2$ (**4b**) as clear, colorless crystals in 78% yield [Equation (1)] and [Equation (2)].

$$[H_2C(PCl_2)_2] + 4\ i\text{PrMgCl} \rightarrow [H_2C(Pi\text{Pr}_2)_2] + 4\ \text{MgCl}_2 \quad (1)$$

$$[H_2C(Pi\text{Pr}_2)_2] + E_{(s)} \rightarrow \text{EP}i\text{Pr}_2\text{CH}_2\text{P}i\text{Pr}_2 \quad (2)$$

X-ray quality crystals of **4a** were obtained by slowly cooling a hot hexanes solution, and the crystal structure is illustrated in Figure 1. Crystals of **4b** were obtained by slow evaporation of a hexanes solution, and the molecular structure is analogous to that of **4a**. Selected bond lengths and bond angles for **4a** and **4b** are given in Table 1.

The monotelluride **4a** crystallizes in the monoclinic space group $P2_1/n$ with four molecules in the unit cell. The hydrogen atoms of the CH_2 group were located from the Fourier density map. Thus, in contrast to the isoelectronic PNP-bridged monotelluride **3a**,[4a] the PCP-bridged analogue **4a** forms the CH_2 tautomer in preference to the PH tautomer in the solid state. The closest intermolecular contact in **4a** is a single Te–H interaction at 2.96 Å to one *i*Pr CH_3 group. The Te–P–C–P dihedral angle in **4a** is 56.1(2)°, whereas the corresponding Te–P–N–P dihedral angle in **3a** is only 3.2(2)°.[4a] The formation of different tautomers for **4a** and **3a** may explain this major structural divergence. The P–Te

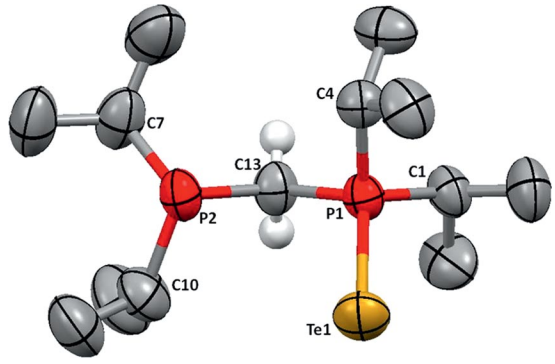

Figure 1. Crystal structure of TeP*i*Pr$_2$CH$_2$P*i*Pr$_2$ (**4a**). Hydrogen atoms of the *iso*-propyl groups have been omitted for clarity. Thermal ellipsoids are shown at 95% probability, H atoms are indicated by spheres of 0.30 Å radius.

Table 1. Selected bond lengths [Å] and bond angles [°] in **4a** and **4b**.

	Bond lengths [Å] **4a** (E = Te)	**4b** (E = Se)
E1–P1	2.3603(7)	2.1155(6)
P1–C13	1.824(3)	1.815(3)
P1–C1	1.841(3)	1.844(3)
P1–C4	1.846(3)	1.815(2)
P2–C7	1.857(3)	1.867(3)
P2–C13	1.868(3)	1.867(2)
P2–C10	1.869(3)	1.858(2)

	Bond angles [°] **4a** (E = Te)	**4b** (E = Se)
P1–C13–P2	111.93(15)	112.05(10)
C13–P1–C1	105.04(13)	103.72(9)
C13–P1–C4	103.59(13)	105.01(9)
C1–P1–C4	108.63(13)	108.54(9)
C13–P1–E1	111.63(10)	111.46(7)
C1–P1–E1	112.95(10)	113.92(6)
C4–P1–E1	114.20(9)	113.39(7)
C7–P2–C13	99.78(13)	99.24(9)
C7–P2–C10	105.67(15)	104.97(9)
C13–P2–C10	99.16(14)	100.56(9)

bond length of 2.3603(7) Å in **4a** is slightly shorter (by ca. 0.02 Å) than that in **3a** and can be compared directly with the value of 2.365 Å reported for *i*Pr$_3$PTe.[9,10] The disparity of 0.044 Å in the P–C bond lengths of the PCP-bridge is attributed to the different oxidation states of the two phosphorus atoms.

The monoselenide **4b** crystallizes in the monoclinic space group $P2_1/c$, also with four molecules in the unit cell. The hydrogen atoms of the CH_2 group were again located from the Fourier density map. The Se–P–C–P dihedral angle in **4b** is 56.7(1)° and an Se–H$_{(i\text{Pr})}$ intermolecular contact is observed with a distance of 2.922 Å. The P–Se bond length of 2.1155(6) Å in **4b**, cf. a value of 2.1212(9) Å found for *i*Pr$_3$PSe.[11]

Computational Studies: P-H and C/N-H Tautomerism

A detailed computational study was carried out in order to explain the solid-state structures of **4a** and **4b** relative to

those of their PNP-bridged analogues **3a** and **3b**. Specifically, the relative stabilities of the PH tautomers compared to the corresponding NH or CH_2 tautomers for the PNP- and PCP-bridged monotellurides were of interest. In calculating the relative total bonding energies of the tautomers of PNP- and PCP-bridged monotellurides, the influence of the substituent on phosphorus and the nature of the chalcogen were also included by performing the calculations for the series $EPR_2CH_2PR_2$ and EPR_2NHPR_2 (R = Me, *i*Pr, *t*Bu, Ph and E = Te, Se) (see **5a**–**h** and **6a**–**h**). The inclusion of R = Ph in these calculations was prompted by the reports that the monochalcogenides $EPPh_2NHPPh_2$ (E = S, Se) exist exclusively as the NH tautomer, both in solution and in the solid state.[12,13]

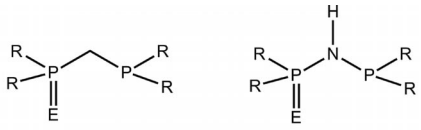

a E = Te, R = Me
b E = Te, R = *i*Pr
c E = Te, R = *t*Bu
d E = Te, R = Ph
e E = Se, R = Me
f E = Se, R = *i*Pr
g E = Se, R = *t*Bu
h E = Se, R = Ph

5

a E = Te, R = Me
b E = Te, R = *i*Pr
c E = Te, R = *t*Bu
d E = Te, R = Ph
e E = Se, R = Me
f E = Se, R = *i*Pr
g E = Se, R = *t*Bu
h E = Se, R = Ph

6

Gas-phase structures of **5a**–**h** and **6a**–**h** and those of the corresponding PH tautomers were optimized. The total bonding energies of these tautomers, as well as the difference in their energies calculated according to Equation (3), are summarized in Table 2.

$$\Delta E = E_{NH/CH_2} - E_{PH} \quad (3)$$

Table 2. Differences in total bonding energy for PH and NH/CH_2 tautomers of **5a**–**h** and **6a**–**h**.[a] All values corrected for zero-point energy.

	ΔE [kJ mol^{-1}] ($E_{CH2} - E_{PH}$)		ΔE [kJ mol^{-1}] ($E_{NH} - E_{PH}$)
5a	–76.1	**6a**	4.8
5b	–59.0	**6b**	23.3
5c	–53.5	**6c**	17.6
5d	–70.5	**6d**	2.9
5e	–77.5	**6e**	0.6
5f	–61.6	**6f**	20.3
5g	–58.1	**6g**	14.6
5h	–72.2	**6h**	–4.5

[a] Compounds **5b**, **6b**, **5f**, **6f** are **4a**, **3a**, **4b**, **3b**, respectively, in the previous section.

The electronic effects of the PCP backbone appear to be very different from those of the PNP fragment. For the series **5a**–**h**, the CH_2 tautomer is more stable than the PH tautomer by more than 53 kJ mol^{-1}. By contrast, the PH tautomer is favored by 18–23 kJ mol^{-1} for the PNP-bridged species when R = *i*Pr, *t*Bu; E = Te, Se, which suggests that the donor ability of the central nitrogen atom is the likely cause of the difference. Although the nature of the backbone is paramount in directing tautomer formation in these isoelectronic systems, the substituents on phosphorus do have a noticeable influence within the PNP-bridged series of compounds. Thus, in contrast to the *i*Pr and *t*Bu derivatives, Me or Ph substituents show only small energy differences of <4.8 kJ mol^{-1} between the two tautomeric forms for E = Te. However, a slight preference (ca. 5 kJ mol^{-1}) for the N–H tautomer is indicated for R = Ph, E = Se, consistent with the experimental observations.[12] Thus, the computational results support the notion that substituents that increase the basicity of the lone pair on the phosphorus atom favor the formation of the PH tautomer in the case of the PNP-bridged systems.[4a] A cogent manifestation of this viewpoint is the predisposition for the PH tautomer in the asymmetrical PNP-bridged system $HP(NMe_2)_2PNPPh_2S$, presumably as a result of the electron-donating Me_2N substituent.[14] In this regard, we also note that electron-withdrawing groups on nitrogen make the NH group more acidic, again favoring the PH form in phosphanylsulfonamide derivatives of the type $RSO_2NHPR'_2$, which have been exploited in catalysis.[15,16]

The different electronic effects of the PCP and PNP backbones are also apparent in the models of the non-chalcogenated species (Table 3). In both cases, regardless of the substituent, the P–H tautomer is always higher in energy, but the magnitude of the energy difference is dependent on the central atom. With a methylene bridge, the CH_2 tautomer is preferred by more than 80 kJ mol^{-1}, while a central N atom provides a much lower energy difference (less than 43 kJ mol^{-1}). These energy barriers are too high for the PH tautomer to be observed in solution, except in the case of *t*Bu substitution. In this case, the energy difference is only 18 kJ mol^{-1}, which is low enough that solvent effects and ambient temperature could allow for both tautomers to co-exist in solution. Indeed, we have previously observed experimentally that a mixture of NH and PH tautomers (ca. 70:30) is present in a toluene solution of this derivative at room temperature.[4b]

Table 3. Differences in energy for PH and NH/CH_2 tautomers of $CH_2(PR_2)_2$ and $HN(PR_2)_2$ (R = Me, *i*Pr, *t*Bu, Ph). All values corrected for zero-point energy.

	ΔE [kJ mol^{-1}] ($E_{CH2} - E_{PH}$)		ΔE [kJ mol^{-1}] ($E_{NH} - E_{PH}$)
$CH_2(PMe_2)_2$	–101.1	$NH(PMe_2)_2$	–42.3
$CH_2(PiPr_2)_2$	–85.5	$NH(PiPr_2)_2$	–29.9
$CH_2(PtBu_2)_2$	–81.5	$NH(PtBu_2)_2$	–18.0
$CH_2(PPh_2)_2$	–102.4	$NH(PPh_2)_2$	–39.7

The influence of the alkyl substituent on the nucleophilicity of the phosphorus center was modeled by comparing the charges on phosphorus. By using the ADF computational package, charges are provided as Mulliken,[17] Hirshfeld,[18] and Voronoi deformation density (VDD) values.[19] Mulliken population analysis results in equal sharing of electron density between centers and is known to exaggerate the charges; Hirshfeld and VDD methods more effectively parse the density and are said to be more accurate.[20] It should be noted that despite these differences, the trends in the data are consistent between the three methods (Table 4).

In each of the systems, the charge on the phosphorus atoms increases modestly with inductive strength of the alkyl group, Me < *i*Pr < *t*Bu. These changes are moderate however, increasing by ca. 0.2 a.u. for Mulliken, 0.03 a.u. for Hirshfeld, and 0.02 a.u. for VDD.

Table 4. Calculated average charges[a] (in a.u.) of phosphorus atoms in $CH_2(PR_2)_2$ and $HN(PR_2)_2$ (R = Me, *i*Pr, *t*Bu, Ph).

	CH_2 Tautomer			PH Tautomer		
	Mulliken	Hirshfeld	VDD	Mulliken	Hirshfeld	VDD
$CH_2(PMe_2)_2$	0.208	0.136	0.050	0.428	0.204	0.162
$CH_2(PiPr_2)_2$	0.301	0.151	0.056	0.634	0.217	0.165
$CH_2(PtBu_2)_2$	0.436	0.175	0.073	0.723	0.228	0.175
$CH_2(PPh_2)_2$	0.253	0.139	0.062	0.527	0.198	0.168
	NH Tautomer			PH Tautomer		
$NH(PMe_2)_2$	0.332	0.169	0.106	0.542	0.232	0.190
$NH(PiPr_2)_2$	0.390	0.176	0.103	0.733	0.254	0.204
$NH(PtBu_2)_2$	0.482	0.199	0.116	0.793	0.268	0.219
$NH(PPh_2)_2$	0.354	0.163	0.110	0.586	0.232	0.204

[a] As a result of differences in the molecular geometry, there is occasionally a slight variation in atomic charge between atoms.

Solution Behavior of $EPiPr_2CH_2PiPr_2$ (4a, E = Te; 4b, E = Se): Multinuclear NMR Spectroscopy Studies

The $^{31}P\{^1H\}$ NMR spectrum of **4a** in [D_8]toluene at 298 K exhibits two broad resonances at 21.1 and –2.6 ppm, which correspond to the P^V and P^{III} centers, respectively; the broadness of the peaks prevented the determination of coupling constants at room temperature. Attempts to determine the ^{125}Te NMR chemical shift at 298 K were also unsuccessful. In the ^1H NMR spectrum, four resonances are observed at 298 K: (a) two independent doublets of doublets at δ = 0.99 and 1.02 ppm, which correspond to the isopropyl CH_3 groups and exhibit coupling to nearby phosphorus [$^3J(^1H,^{31}P)$ = 15 Hz] and hydrogen nuclei [$^3J(^1H,^1H)$ = 7.0 Hz], (b) a partially resolved broad resonance at δ = 1.85 ppm, which can be attributed to CH hydrogen atoms of the four isopropyl groups, and (c) a pseudo-triplet at δ = 1.93 ppm, which results from the coupling of CH_2 protons in the PCP backbone to the two phosphorus nuclei [$^2J(^1H,^{31}P)$ = 6 Hz]; the coupling of these protons to the two phosphorus nuclei appears to be equivalent at room temperature. In summary, the multinuclear NMR spectroscopy data for **4a** clearly indicate fluxional behavior in solution.

In order to probe the nature of this exchange process, we carried out a multinuclear (^1H, ^{31}P and ^{125}Te) NMR study of **4a** in [D_8]toluene over the temperature range 218–338 K. In the $^{31}P\{^1H\}$ NMR spectrum, the two broad resonances observed at room temperature sharpen markedly with lower temperatures (Figure 2a), and at 218 K the $^2J(^{31}P,^{31}P)$ couplings (63 Hz) and ^{125}Te satellites are clearly visible $^1J(^{31}P,^{125}Te)$ = 1735 Hz (cf. 1735 Hz for iPr_3PTe) (Figure 2b).[9] This value was corroborated by the ^{125}Te NMR spectrum at 218 K, which exhibits a well-resolved doublet with $^1J(^{31}P,^{125}Te)$ = 1734 Hz; however, upon warming the solution, this doublet collapses and is lost in the baseline at 258 K. There was no evidence for the existence of the PH tautomer in solution throughout the temperature range.

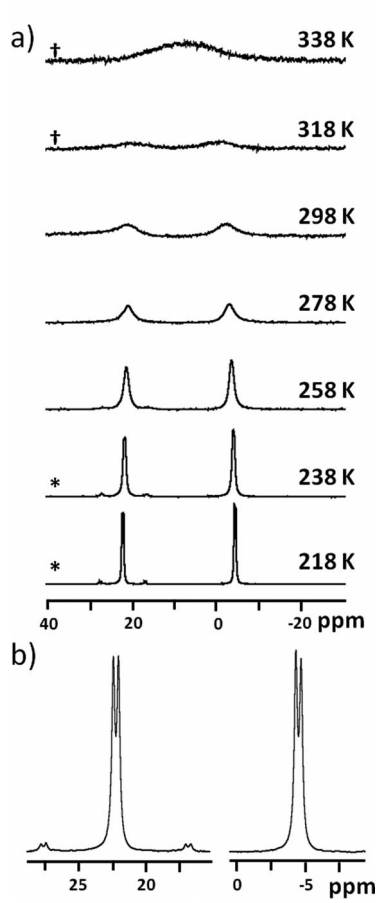

Figure 2. Variable-temperature ^{31}P NMR spectra for $TePiPr_2CH_2PiPr_2$ (**4a**) in [D_8]toluene (a) in the temperature range 218–338 K (* = shown at 1/2 vertical scale, † = shown at 4× vertical scale), and (b) expansion of the 218 K spectrum to show P–P coupling.

In the ^1H NMR spectrum, cooling of the sample to 218 K results in a deceleration of the exchange process on the NMR time scale. As illustrated in Figure 3, the triplet corresponding to the CH_2 resonance begins to separate into a doublet at δ = 1.69 ppm, while the previously poorly resolved isopropyl C–H resonance separates into two distinctly different broad resonances centered at δ = 1.59 and 1.98 ppm. When the solution is heated, these two resonances collapse to give a broad resonance at 278 K, which becomes well-resolved to reveal couplings to the CH_3 hydrogen atoms at 338 K. Interestingly, the resonances corresponding to the isopropyl CH_3 protons approach equivalence upon heating. Whereas below room temperature the two different resonances for the isopropyl CH_3 groups on the P^{III} and P^V centers are easily differentiated, their positions and intensities are nearly identical at 338 K ($\Delta\delta$ = 9.0 Hz). Upon cooling, this equivalence is again lost, and at 238 K one set has almost completely broadened into the baseline. It is expected that at these low temperatures, bond rotations may be slow on the NMR timescale, which leads to a notable inequivalence of the isopropyl groups on the P^{III} and P^V centers.

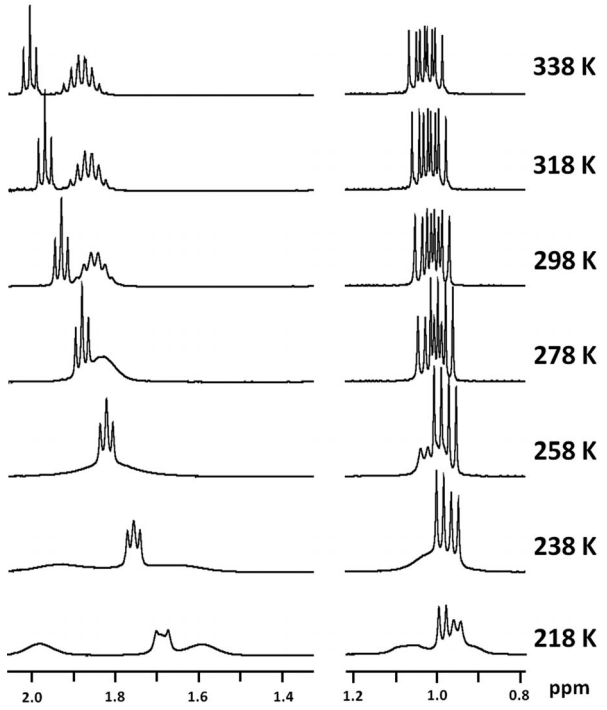

Figure 3. Variable-temperature ^{1}H NMR spectra for TeP*i*Pr$_2$CH$_2$-P*i*Pr$_2$ (**4a**) in [D$_8$]toluene in the temperature range 218–348 K. The portion of the spectra corresponding to CH$_3$ groups is presented at 1/2 vertical scale.

In summary, the variable temperature NMR spectroscopy data are consistent with an exchange process that is rapid on the NMR time scale at room temperature. We note that the ^{125}Te NMR spectra of the phosphane tellurides R$_3$PTe (R = *n*Bu, *t*Bu, Ph[21]) are observed to collapse from a well-resolved doublet into a broad resonance in the presence of excess R$_3$P.[22] In the case of **4a**, the presence of the P^{III} center could provide the site for tellurium exchange between the two phosphorus centers through either an inter- or an intramolecular process.

In order to differentiate between these two exchange pathways, a VT-NMR study was undertaken, in which the concentration was also varied; an intermolecular process is expected to exhibit concentration dependence, which would not be evident for intramolecular exchange. ^{31}P{^{1}H} NMR spectra of four solutions involving one-half serial dilutions of a 0.053 ± 0.002 mol L^{-1} sample were collected over the temperature range 215–355 K. It was immediately apparent that, although the chemical shifts were unaffected by the concentration, the broadness of the resonances, and hence the rate of exchange, was affected; the most concentrated sample showed two broad resonances at room temperature, but with lower concentrations, the peaks sharpened significantly.

The rate of exchange for each sample at a specific temperature can be approximated by using the full-widths at half-maximum (FWHM) of the P^{III} or P^V resonance [Equation (4)].[23] For the purposes of this analysis, the P^{III} resonance was used, because of the sharper line-shapes in the intermediate temperature range. A linear relationship between the observed rate and the concentrations of **4a** indicates a first-order reaction with respect to **4a** (Table 5). An Arrhenius plot (Figure 4) was thus used to determine an activation energy of 21.9 ± 3.2 kJ mol^{-1} for this process.

$$Rate = k[\mathbf{4a}] = \pi(FWHM - FWHM_0) \quad (4)$$

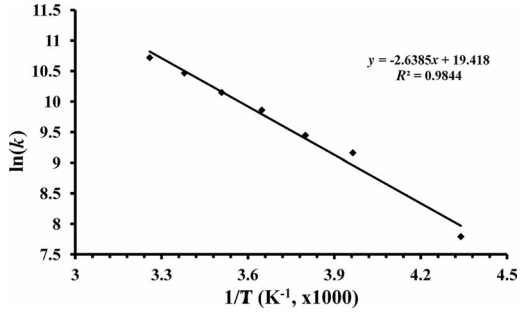

Figure 4. Experimental Arrhenius plot for the Te-transfer process observed in **4a** between 230 and 307 K.

The behavior of the selenium derivative SeP*i*Pr$_2$CH$_2$P*i*Pr$_2$ (**4b**) in solution is more straightforward than that of **4a**. At 298 K, the ^{31}P{^{1}H} NMR spectrum in [D$_8$]toluene exhibits two narrow, well-separated doublets at 57.8 and –4.8 ppm, which correspond to the P^V and P^{III} centers, respectively; each resonance is mutually coupled [^2J(^{31}P,^{31}P) = 49 Hz], and ^{77}Se satellites are clearly visible on the P^V center [^1J(^{31}P,^{77}Se) = 720 Hz, cf. 708 Hz for *i*Pr$_3$PSe].[11] The ^{77}Se NMR chemical shift is observed at –429.6 ppm at this same temperature (cf. –489.9 ppm for *i*Pr$_3$PSe).[11] and exhibits the same ^1J coupling to phosphorus. In the ^{1}H NMR spectrum, the following resonances are observed: (a) two independent doublets of doublets at δ = 1.01 and 1.06 ppm, which correspond to the isopropyl CH$_3$ groups, exhibit coupling to nearby phosphorus [^3J(^{1}H,^{31}P) = 17 Hz] and hydrogen nuclei [^3J(^{1}H,^{1}H) = 7.0 Hz], (b) a multiplet at δ = 1.91 ppm, which can be attributed to the four CH hydrogen atoms of the four isopropyl groups, and (c) an apparent

Table 5. Experimentally determined rate data for the Te-transfer process observed in **4a** between 230 and 307 K.

Concentration [mol L^{-1}]	Rate [s^{-1}] 230 K	Rate [s^{-1}] 252 K	Rate [s^{-1}] 263 K	Rate [s^{-1}] 274 K	Rate [s^{-1}] 285 K	Rate [s^{-1}] 296 K	Rate [s^{-1}] 307 K
0.003	10	100	99	113	137	142	225
0.007	13	74	93	148	174	215	329
0.013	22	123	160	241	401	499	625
0.027	107	272	457	507	763	1066	1224
0.053	110	493	612	1019	1300	1794	2384
k (L mol^{-1} s^{-1})	2419	9521	12671	19169	25565	35102	45268

doublet at δ = 1.76 ppm, which corresponds to the CH_2 protons in the PCP backbone.

The latter observation represents a notable difference compared to the corresponding signal for **4a**, which was only partially resolved into a pseudo-doublet at 218 K (Figure 3). This disparity may arise from the rapid tellurium exchange that occurs for **4a** at ambient temperature. Selective $^1H\{^{31}P\}$ decoupling experiments for **4a** at room temperature resulted in a collapse of the triplet to a single peak, which suggests that the coupling to the two phosphorus atoms is indeed averaged at room temperature. Similar experiments for **4b**, where there is no apparent fluxionality at 298 K, led to a partial collapse of the doublet when the P^V center was decoupled. Decoupling of the P^{III} center led to no visible change in the shape of the CH_2 resonance. These data suggest that the doublet is in fact a doublet of doublets, which exhibits a large coupling to P^V [$^2J(^1H,^{31}P)$ = 12 Hz] and a very small coupling to P^{III} (could not be measured). It then follows that in the absence of exchange, **4a** should also exhibit this coupling pattern.

Although the multinuclear NMR spectroscopy data for **4b** do not immediately suggest fluxional behavior in solution at room temperature, evidence of a slow exchange process was apparent from the line-broadening observed in the $^{31}P\{^1H\}$ NMR spectra collected over the temperature range 298–355 K. The nature of this exchange is likely comparable to that of **4a**, but **4b** exhibits a much higher activation barrier as the peaks do not approach equivalence as in **4a**. It is expected that this is a result of the more electronegative Se atom and a stronger P–Se bond than the P–Te bond.[24]

In an attempt to evaluate the influence of the phosphorus substituents on the energy barriers for chalcogen exchange, the synthetic procedure outlined in Equations (1) and (2) was applied to the synthesis of the tetramethyl derivative $TePMe_2CH_2PMe_2$. Surprisingly, the methyl-substituted PCP-bridged precursor $Me_2PCH_2PMe_2$, which was obtained as a clear, colorless liquid,[25] failed to react with either elemental tellurium or the tellurium-transfer reagents R_3PTe (R = Et, *t*Bu)[26] even in boiling toluene. By comparison with the high-yield synthesis of **4a**, the lack of formation of the monotelluride $TeMe_2PCH_2PMe_2$ under these conditions is puzzling, especially in the light of a literature report that describes the ditelluration of $Me_2PCH_2CH_2PMe_2$ with Et_3PTe in toluene at room temperature to give $TePMe_2CH_2CH_2PMe_2Te$ in 51% yield.[27] Unfortunately, it was not possible to extend this investigation to the *tert*-butyl derivative $Te\mathit{t}Bu_2PCH_2P\mathit{t}Bu_2$ because the reaction of $H_2C(PCl_2)_2$ with *tert*-butylmagnesium chloride produces the six-membered ring 1,4-$(CH_2)_2(P\mathit{t}Bu)_4$ through a reductive coupling process rather than the expected acyclic product $\mathit{t}Bu_2PCH_2P\mathit{t}Bu_2$.[28,29]

Models of Tellurium Exchange

To compliment these experimental studies, a series of calculations were performed in an attempt to model the reaction pathway for the tellurium transfer in **4a**. On the basis of the experimentally observed concentration dependence, the exchange must occur between two molecules, but, as a comparison, the energetic pathway for intramolecular tellurium exchange was considered first. An intramolecular tellurium-transfer model was calculated by varying the difference of the d_2 and d_1 distances [Scheme 1, defined as x in Equation (5)] in 0.2 Å steps from x = –2.2 Å to 2.2 Å. A plot of the potential energy at each value of x (Figure 5) indicates one energetic maximum at x = 0 and two energy wells when x is equal to 1.8 Å and –1.8 Å (representing the two isomers of **4a**). The maximum has an energy of 168 kJ mol^{-1} relative to the minimum, well beyond what could be achieved in the temperature range studied experimentally. At the minima on the curve, the long P–Te distance of 4.20 Å [Σ_{vdw}(P,Te) = 4.05 Å] suggests that there is no intramolecular bonding contribution to the intermolecular Te transfer.

$$d_2 - d_1 = x \quad (5)$$

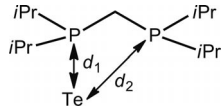

Scheme 1.

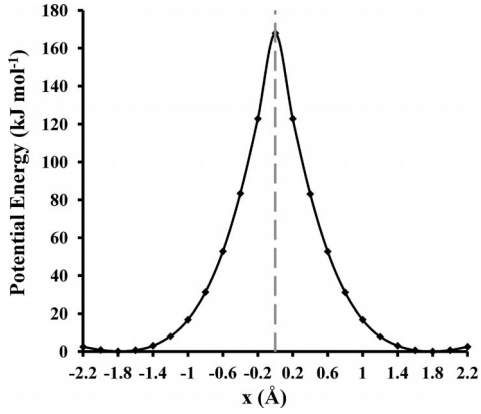

Figure 5. Potential energy curve for a possible intramolecular Te-transfer process in **4a**. (--- indicates x = 0 Å).

A simple intermolecular transfer model would involve a single point of attachment between two molecules of **4a**. As a first approximation, the difference in the distances d_2 and d_1 [Scheme 2, defined as x in Equation (5)] was varied in 0.1 Å steps between x = –1.4 Å and 1.4 Å, with all other geometric parameters allowed to optimize at each step. In this manner, an approximation of the intermolecular transfer pathway was made. A plot of the total bonding energy showed two well-defined minima, and a single maximum. By using the molecular geometries at these points, the structures were reoptimized without constraints (but with tighter convergence criteria and a higher integration accuracy) to provide more accurate structures and energies; a transition-

state search for the geometry at the maximum was used to model the activation barrier. The energies and values for x at these points are shown in Figure 6.

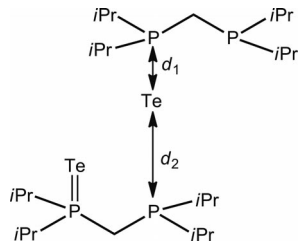

Scheme 2.

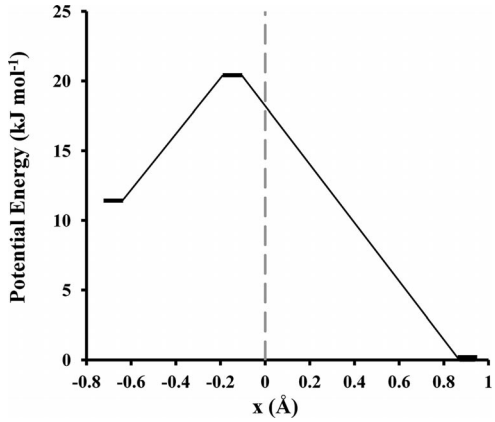

Figure 6. Energy diagram for the intermolecular Te-transfer process in **4a**. (--- indicates x = 0 Å).

The minima can best be described as a dimer of **4a** (where x = 0.905 Å) and an adduct of $CH_2(PiPr_2)_2$ and $CH_2(PiPr_2Te)_2$ (where x = –0.685 Å), while the maximum (where x = –0.147 Å) represents a transition state where the Te atom is bridged between molecules (Figure 7). The P1–Te1–P2 bond angles (176.2° for structure a, 177.4° for structure b and 176.8° for structure c) are all in good agreement with the solid-state structure of $(Ph_3P)_2Te$, which exhibits a 180° P–Te–P angle.[21] Although the presence of a second tellurium atom is expected to have an effect on the calculated energies, the observation that the P–Te2 bond length and the Te2–P–C–P dihedral angle remain unchanged throughout the reaction pathway indicates that such a perturbation is relatively minor.

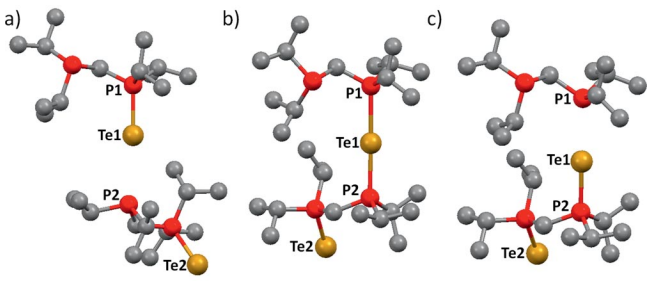

Figure 7. Optimized structures of (a) the dimer of **4a**, (b) the transition state for tellurium transfer, and (c) the $CH_2(PiPr_2)_2$/$CH_2(PiPr_2Te)_2$ adduct.

The dimeric structure (Figure 7a) is lower in energy by 11.4 kJ mol^{-1} when compared to the $CH_2(PiPr_2)_2$/$CH_2(PiPr_2Te)_2$ adduct (Figure 7c). The calculated energetic barrier for transfer of the tellurium atom to a second molecule is 20.4 kJ mol^{-1}, while that for the reverse reaction is 9.1 kJ mol^{-1}. This suggests that, although the dimer of **4a** is preferred, conversion between the two minima would be expected in solution at room temperature. This energy barrier correlates very well with the experimentally observed E_a of 21.9 ± 3.2 kJ mol^{-1}, which suggests that this is indeed the transfer process observed in the NMR experiments. This model, however, is inconsistent with the experimentally observed coalescence of the two ^{31}P resonances, as such a model would require all phosphorus environments to be the same as a result of the transfer. This discrepancy could be accounted for by the occurrence of multiple intermolecular Te-exchange processes that would give rise to a single ^{31}P NMR chemical shift.

Consideration of a simple dimer with two points of attachment (Scheme 3) gave intermolecular P–Te bond lengths well in excess of the sum of van der Waals radii (4.116, 4.354 Å). This result seems to rule out a symmetrical intermediate in the exchange process. A contraction of the molecular Te–P–C–P dihedral angle required to achieve this geometry (ca. 60° relative to 90° in the free molecule) likely contributes to the long P–Te distances. Consequently, a more accurate model should be sufficiently large to allow for a more relaxed geometry. Such an extended system, however, is beyond our computational resources at this time.

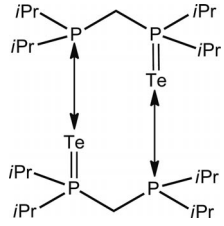

Scheme 3.

Reactions of 4a with Chalcogens and *n*BuLi

In our previous attempts to sequentially oxidize the two P^{III} centers in $HN(PiPr_2)_2$ with different chalcogens, only one of the P^{III} centers could be oxidized.[5] For comparison, we attempted to prepare a mixed-chalcogen ligand by reaction of **4a** with elemental selenium in toluene at room temperature. The occurrence of a reaction under these conditions was readily evident from the formation of a precipitate of tellurium. However, the ^{31}P NMR spectrum of the supernatant revealed the formation of the known diseleno derivative $H_2C(PiPr_2Se)_2$,[8] in addition to unreacted **4a**, which demonstrates the lability of the P–Te bond in **4a**. Attempts to prepare the ditelluro derivative $TePiPr_2CH_2PiPr_2Te$ by reaction of $iPr_2PCH_2PiPr_2$ with 2.2 equiv. tellurium in boiling toluene for 4 d gave only the monotelluride **4a**; the Te-

transfer reagents Et_3PTe or tBu_3PTe were also ineffective in oxidizing the second P^{III} center.

A second manifestation of the lability of the P–Te bond in **4a** was provided by the attempted lithiation of **4a** with *n*BuLi in THF at –78 °C, followed by warming to room temperature. Under these conditions, the only detectable product in the ^{31}P NMR spectrum was the P^{III}/P^{III} precursor $H_2C(PiPr_2)_2$, presumably formed as a result of cleavage of the P–Te bond.

Conclusions

In contrast to their PNP-bridged analogues, the PCP-bridged monochalcogenides $EPiPr_2CH_2PiPr_2$ (E = Te, Se) exist as the CH_2 tautomer in the solid state. DFT calculations provide support for the higher stability of the PH tautomer in the case of the alkyl-substituted PNP-bridged monochalcogenides, **6b**, **6c**, **6f**, and **6g**, and indicate that this preference can be attributed to the different electronic effects of the PNP relative to PCP bridge. In solution, however, the monotelluride **4a** undergoes a rapid intermolecular tellurium exchange with an activation energy of ca. 22 kJ mol^{-1} as determined by NMR spectroscopy studies supported by DFT calculations. In contrast, the monoselenide, **4b**, undergoes slow exchange, likely because of a much larger activation energy. Although the lability of the P–Te bond in **4a** preempts the direct formation of a lithium derivative for metathesis reactions, the coordination chemistry of the neutral ligands **4a** and **4b**, which incorporate both heavy chalcogen and P^{III} donor centers, merits detailed investigation.

Experimental Section

Reagents and General Procedures: All reactions and the manipulation of products were performed under an atmosphere of argon by using standard Schlenk techniques. The compounds $[H_2C(PCl_2)_2]$ (Strem Chemicals, >90%), MeMgCl (Aldrich, 3.0 M solution in THF), *i*PrMgCl (Aldrich, 2.0 M solution in THF), *t*BuMgCl (Aldrich, 1.0 M solution in THF), *n*BuLi (Aldrich, 2.5 M solution in hexanes), and elemental Te (Aldrich, 30 mesh, 99.997%), and Se (Aldrich, 200 mesh, 99.5+%) were used as received. The solvents *n*-hexane, toluene, diethyl ether, and THF were dried by distillation over sodium/benzophenone under an argon atmosphere prior to use. Samples of Et_3PTe[30] and tBu_3PTe[31] were synthesized according to literature procedures. The compound $H_2C(PMe_2)_2$ was obtained as a clear, colorless, highly air-sensitive liquid from the reaction of $[H_2C(PCl_2)_2]$ with MeMgCl in diethyl ether according to the literature procedure and was shown to be pure by NMR spectroscopy [δ $^{31}P(^1H)$ = –55.0 (s) in reagent toluene, lit. value –55.8].[25] Elemental analyses were performed on a Perkin Elmer 2400 elemental analyzer equipped to measure C, H and N.

Spectroscopy Methods: The ^1H, ^{13}C, ^{31}P, ^{77}Se, and ^{125}Te NMR spectra were obtained in [D_8]toluene between 218–338 K on a Bruker DRX 400 spectrometer operating at 399.46, 100.46, 161.71, 76.13, and 125.90 MHz, respectively. ^1H and ^{13}C-DEPT135 NMR spectra are referenced to the solvent signal, and the chemical shifts are reported relative to $(CH_3)_4Si$. ^{13}C δ chemical shift assignments were confirmed by using 2D techniques (HSQC and HMBC). ^{31}P spectra are referenced externally to an 85% solution of H_3PO_4 at 0 ppm, ^{77}Se spectra to an external reference of Ph_2Se_2 in $CDCl_3$ at δ = 463 ppm, and ^{125}Te spectra to Ph_2Te_2 in $CDCl_3$ at δ = 422 ppm. Mass spectra (EI/CI) were obtained with a Thermo Finnigan SSQ7000 mass spectrometer with a direct insertion probe.

X-ray Crystallography: Crystallographic data for **4a** and **4b** are summarized in Table 6. Crystals of **4a** and **4b** were coated with Paratone 8277 oil and mounted on a nylon loop. Diffraction data were collected on a Nonius KappaCCD diffractometer by using monochromated Mo-K_α radiation (λ = 0.71073 Å) at –150 °C (**4a**) and –100 °C (**4b**). An absorption correction was applied during the data collection by using the SORTAV program.[32] The structures were solved by direct methods by using SHELXS-97 and refined by using SHELXL-97.[33,34] After full-matrix least-squares refinement of the non-hydrogen atoms with anisotropic thermal parameters, the hydrogen atoms were placed in idealized locations by using the appropriate riding models. The locations of the hydrogen atoms bonded to the PCP carbon atom were located from the Fourier density map and were refined.

Table 6. Crystallographic data for **4a** and **4b**.

	4a	**4b**
Empirical formula	$C_{13}H_{30}P_2Te$	$C_{13}H_{30}P_2Se$
Formula weight	375.91	327.27
Crystal system	monoclinic	monoclinic
Space group	$P2_1/n$	$P2_1/c$
a [Å]	10.7740(4)	10.7760(3)
b [Å]	11.9480(2)	11.7200(3)
c [Å]	14.0990(5)	14.2610(5)
α [°]	90.00	90.00
β [°]	107.8230(11)	114.7410(11)
γ [°]	90.00	90.00
V [Å^3]	1727.83(9)	1677.06(7)
Z	4	4
T [°]C	–150	–100
$\rho_{calcd.}$ [mg/m^3]	1.445	1.296
μ(Mo-K_α) [mm^{-1}]	1.886	2.409
Crystal size [mm^3]	0.19 × 0.11 × 0.07	0.12 × 0.10 × 0.08
F(000)	760	688
θ Range [°]	2.1–27.40	2.32–27.55
No. of reflections collected	6630	14118
No. of unique reflections	3698	3854
R_{int}	0.0246	0.0336
no. of reflections [$I > 2\sigma(I)$]	3450	3396
$R1$ [$I > 2\sigma(I)$]	0.0311	0.0293
$wR2$ (all data)	0.0726	0.0687
GOF on F^2	1.127	1.057
Completeness	0.982	0.991

CCDC-910200 and -910201 contain the supplementary crystallographic data for this paper. These data can be obtained free of charge from The Cambridge Crystallographic Data Centre via www.ccdc.cam.ac.uk/data_request/cif.

Computational Details: The structures considered in these studies were optimized by using the ADF DFT package, version 2012.01.[35–37] The adiabatic local density approximation (ALDA) was used for the exchange-correlation kernel,[38,39] and the differentiated static LDA expression was used with the Vosko–Wilk–Nusair parameterization.[40] Calculations of model geometries were gradient corrected with the exchange and correlation functionals proposed in 1991 by Perdew and Wang (PW91).[41,42] The structures were refined by using a triple-ζ all-electron basis set with two polarization functions and by applying the zeroth order regular approximation (ZORA)[43–47] formalism with the specially adapted basis

sets. The validity of all optimized structures was confirmed by using frequency calculations; all calculated energies have been corrected for zero-point energies and basis set superposition error where applicable.

Synthesis of TeP*i*Pr$_2$CH$_2$P*i*Pr$_2$ (4a): A solution of [H$_2$C(PCl$_2$)$_2$] (0.953 g, 4.38 mmol) in THF (30 mL) was cooled to –78 °C prior to the addition of *i*PrMgCl (9.6 mL of a 2.0 M solution in THF) dropwise by syringe. The reaction mixture was stirred for 1 h at –78 °C, 30 min at 23 °C, and finally heated for 3 h at 50 °C. The solvent was removed under vacuum, and the oily product was extracted with ca. 40 mL of Et$_2$O. The solution was passed through a PTFE disk to remove solid MgCl$_2$, the solvent was removed under vacuum, and the sample of [H$_2$C(P*i*Pr$_2$)$_2$] was redissolved in toluene (30 mL). This solution was then transferred into a flask containing elemental tellurium (0.619 g, 4.85 mmol) and was heated at reflux for 21 h. Once cooled, this solution was filtered through a PTFE disk to remove unreacted tellurium. Solvent removal resulted in a yellow solid, which was extracted repeatedly with hexanes to yield **4a** as a pale yellow powder (1.595 g, 4.27 mmol, 98%). M.p. 95–98 °C. C$_{13}$H$_{40}$P$_2$Te (395.91): calcd. C 41.50, H 8.00; found C 41.57, H 7.94. ^{1}H NMR ([D$_8$]toluene, 23 °C): δ = 1.93 [t, ^2J(^{1}H,^{31}P) = 6 Hz, 2 H, CH of the PCP carbon], 1.85 [m, 4 H, C*H*(CH$_3$)$_2$], 1.02 [dd, ^3J(^{1}H, ^{1}H) = 7, ^3J(^{1}H,^{31}P) = 15 Hz, 12 H, CH(C*H*$_3$)$_2$ on P^V], 0.99 [dd, ^3J(^{1}H, ^{1}H) = 7, ^3J(^{1}H,^{31}P) = 14 Hz, 12 H, CH(C*H*$_3$)$_2$ on P^{III}] ppm. ^{1}H NMR ([D$_8$]toluene, –55 °C): δ = 1.98 [m, 2 H, C*H*(CH$_3$)$_2$ on P^V], 1.69 [d, ^2J(^{1}H,^{31}P) = 12 Hz, 2 H, CH$_2$ of the PCP carbon], 1.59 [m, 2 H, C*H*(CH$_3$)$_2$ on P^{III}], 1.06 [br. m, 12 H, CH(C*H*$_3$)$_2$ on P^V], 0.96 [dd, ^3J(^{1}H, ^{1}H) = 7, ^3J(^{1}H,^{31}P) = 14 Hz, 12 H, CH(C*H*$_3$)$_2$ on P^{III}] ppm. ^{13}C-DEPT135 NMR (25 °C): δ = 19.9 (br. s, 1C, C of PCP), 19.8 [br. s, 4C, *C*H(CH$_3$)$_2$], 18.9 [br. s, 8C, CH(*C*H$_3$)$_2$] ppm. ^{31}P{^{1}H} NMR (23 °C): δ = 21.1 (br. s, 1 P, P^V), –2.6 (br. s, 1 P, P^{III}) ppm. ^{31}P{^{1}H} NMR (–55 °C): δ = 22.2 [d, ^2J(^{31}P,^{31}P) = 60, ^1J(^{31}P,^{125}Te) = 1735 Hz, 1 P, P^V], –2.6 [d, ^2J(^{31}P,^{31}P) = 60 Hz, 1 P, P^{III}] ppm. ^{125}Te NMR (–55 °C): δ = –940.29 [d, ^1J(^{125}Te,^{31}P) = 1735 Hz] ppm. X-ray quality crystals of **4a** were obtained by dissolving a sample in hot hexanes, then allowing the solution to cool slowly in a warm water bath.

Synthesis of SeP*i*Pr$_2$CH$_2$P*i*Pr$_2$ (4b): The reagent [H$_2$C(P*i*Pr$_2$)$_2$] was prepared from [H$_2$C(PCl$_2$)$_2$] (0.403 g, 1.85 mmol) and *i*PrMgCl (3.8 mL of a 2.0 M solution in THF) and isolated as described above for the synthesis of **4a**. A solution of [H$_2$C(P*i*Pr$_2$)$_2$] (1.85 mmol) in toluene (30 mL) was then cooled to 0 °C and transferred into a flask containing a rapidly stirred slurry of elemental selenium (0.145 g, 1.84 mmol) in toluene (5.0 mL), also at 0 °C. This mixture was then warmed slowly to room temperature with stirring over 21 h. The reaction mixture was then filtered through a PTFE disk to remove unreacted selenium. ^{31}P{^{1}H} NMR spectroscopy of this crude reaction mixture showed complete conversion to monosubstitution, with ca. 6% diselenide SeP*i*Pr$_2$CH$_2$-P*i*Pr$_2$Se as a minor impurity. The solvent was removed from the reaction mixture, and the residue was redissolved in hexanes. Slow evaporation of the solvent resulted in precipitation of clear, colorless crystals of **4b** (0.467 g, 1.43 mmol, 78%). M.p. 68–70 °C. C$_{13}$H$_{40}$P$_2$Se (327.27): calcd. C 47.71, H 9.24; found C 48.26, H 9.07. ^{1}H NMR ([D$_8$]toluene, 25 °C): δ = 1.91 [m, 4 H, C*H*(CH$_3$)$_2$], 1.76 [d, ^2J(^{1}H,^{31}P) = 12 Hz, 1 H, CH$_2$], 1.06 [dd, ^3J(^{1}H, ^{1}H) = 7, ^3J(^{1}H,^{31}P) = 17 Hz, 12 H, CH(C*H*$_3$)$_2$ on P^V], 1.01 [dd, ^3J(^{1}H, ^{1}H) = 7, ^3J(^{1}H,^{31}P) = 16 Hz, 12 H, CH(C*H*$_3$)$_2$ on P^{III}] ppm. ^{13}C-DEPT135 NMR (25 °C): δ = 28.4 [dd, ^1J(^{13}C, ^{31}P) = 42, ^3J(^{13}C, ^{31}P) = 2 Hz, 2 C, CH$_3$ on P^V], 24.3 [dd, ^1J(^{13}C, ^{31}P) = 18, ^3J(^{13}C, ^{31}P) = 7 Hz, 2 C, CH$_3$ on P^{III}], 20.0 [d, ^1J(^{13}C, ^{31}P) = 39 Hz, 1 C, C of PCP], 19.0 [d, ^1J(^{13}C, ^{31}P) = 11 Hz, 4 C, CH$_3$ on P^V], 19.0 [d, ^2J(^{13}C, ^{31}P) = 29 Hz, 4 C, CH$_3$ on P^{III}] ppm. ^{31}P{^{1}H} NMR (25 °C): δ = 57.8 [s, ^1J(^{31}P, ^{77}Se) = 720 Hz, ^2J(^{31}P,^{31}P) = 50 Hz, 1 P, P^V], –4.8 [s, ^2J(^{31}P,^{31}P) = 50 Hz, 1 P, P^{III}] ppm. ^{77}Se NMR (25 °C): δ = –429.6 [d, ^1J(^{77}Se, ^{31}P) = 720 Hz] ppm.

Reaction of 4a with Selenium: A solution of **4a** (0.101 g, 0.26 mmol) in toluene (5 mL) was transferred onto elemental selenium (0.021 g, 0.26 mmol) and stirred with reflux for 18 h. Once the stirring was stopped, extruded tellurium was allowed to settle, and a ^{31}P NMR spectrum of the supernatant solution showed a mixture of **4a** and the diseleno-substituted species H$_2$C(P*i*Pr$_2$Se)$_2$ [δ = 57.3, ^1J(^{31}P,^{77}Se) = 725 Hz], lit. values [δ = 56.8, ^1J(^{31}P,^{77}Se) = 726 Hz in [D$_8$]THF].[8]

Reaction of 4a with *n*BuLi: *n*BuLi (0.23 mL of a 2.5 M solution in THF) was added dropwise with stirring to a solution of **4a** (0.211 g, 0.56 mmol) in THF (10 mL) cooled to –78 °C. The reaction mixture was stirred at this temperature for 30 min and then warmed to room temperature over 1 h. A ^{31}P NMR spectrum of the resulting solution showed only the parent P^{III}/P^{III} compound H$_2$C(P*i*Pr$_2$)$_2$ (δ = –1.6 in toluene), lit. value: δ = –1.3 in [D$_8$]THF.[8]

Acknowledgments

We thank the Natural Sciences and Engineering Council of Canada (NSERC) for continuing financial support. We would also like to acknowledge Drs. M. Krykunov and M. Seth for their invaluable advice regarding ADF methods. We are grateful to Prof. T. Ziegler for access to computational resources.

[1] For a review, see T. Chivers, J. S. Ritch, S. D. Robertson, J. Konu, H. M. Tuononen, *Acc. Chem. Res.* **2010**, *43*, 1053.
[2] For a review, see J. S. Ritch, T. Chivers, M. Afzaal, P. O'Brien, *Chem. Soc. Rev.* **2007**, *36*, 1622.
[3] For specific examples, see a) Sb$_2$Te$_3$: S. S. Garje, D. J. Eisler, J. S. Ritch, M. Afzaal, P. O'Brien, T. Chivers, *J. Am. Chem. Soc.* **2006**, *128*, 3120; b) PbTe: J. S. Ritch, T. Chivers, K. Ahmad, M. Afzaal, P. O'Brien, *Inorg. Chem.* **2010**, *49*, 1198; c) CdTe: K. Ahmad, M. Afzaal, J. S. Ritch, T. Chivers, P. O'Brien, *J. Am. Chem. Soc.* **2010**, *132*, 5964.
[4] a) T. Chivers, D. J. Eisler, J. S. Ritch, H. M. Tuononen, *Angew. Chem.* **2005**, *117*, 5033; *Angew. Chem. Int. Ed.* **2005**, *44*, 4953; b) J. S. Ritch, T. Chivers, D. J. Eisler, H. M. Tuononen, *Chem. Eur. J.* **2007**, *13*, 4643.
[5] S. D. Robertson, T. Chivers, *Dalton Trans.* **2008**, 1765.
[6] a) J. S. Ritch, T. Chivers, *Dalton Trans.* **2008**, 957; b) J. S. Ritch, T. Chivers, *Inorg. Chem.* **2009**, *48*, 3857.
[7] M. Lusser, P. Peringer, *Inorg. Chim. Acta* **1987**, *127*, 151.
[8] J. Konu, H. M. Tuononen, T. Chivers, *Inorg. Chem.* **2009**, *48*, 11788.
[9] N. Kuhn, G. Henkel, H. Schumann, R. Fröhlich, *Z. Naturforsch. B* **1990**, *45*, 1010.
[10] Values in the range 2.288(5)–2.368(4) Å have been reported for a variety of phosphane tellurides. G. G. Briand, T. Chivers, M. Parvez, G. Schatte, *Inorg. Chem.* **2003**, *42*, 525, and references therein.
[11] C. G. Hrib, F. Ruthe, E. Seppälä, M. Bätcher, C. Druckenbrodt, C. Wismach, P. G. Jones, W.-W. du Mont, V. Lippolis, F. A. Devillanova, M. Bühl, *Eur. J. Inorg. Chem.* **2006**, 88.
[12] P. Bhattacharyya, A. M. Z. Slawin, D. J. Williams, J. D. Woollins, *J. Chem. Soc., Dalton Trans.* **1995**, 3189.
[13] P. Bhattacharyya, A. M. Z. Slawin, M. B. Smith, J. D. Woollins, *Inorg. Chem.* **1996**, *35*, 3675.
[14] A. Schmidpeter, H. Rossknecht, *Angew. Chem.* **1969**, *81*, 572; *Angew. Chem. Int. Ed. Engl.* **1969**, *8*, 614.
[15] a) T. León, M. Parera, A. Roglans, A. Riera, X. Verdaguer, *Angew. Chem.* **2012**, *124*, 7057; *Angew. Chem. Int. Ed.* **2012**, *51*, 6951; b) M. Revés, C. Ferrer, T. León, S. Doran, P. Etayo,

A. Vidal-Ferran, A. Riera, X. Verdaguer, *Angew. Chem.* **2010**, *122*, 9642; *Angew. Chem. Int. Ed.* **2010**, *49*, 9452.
[16] F. W. Patureau, S. de Boer, M. Kuil, J. Meeuwissen, P. A. R. Breuil, M. A. Siegler, A. L. Spek, A. J. Sandee, B. de Bruin, J. N. H. Reek, *J. Am. Chem. Soc.* **2009**, *131*, 6683 and references cited therein.
[17] R. S. Mulliken, *J. Chem. Phys.* **1955**, *23*, 2343.
[18] A. E. Reed, L. A. Curtiss, F. Weinhold, *Chem. Rev.* **1985**, *83*, 899.
[19] C. Fonseca Guerra, J.-W. Handgraaf, E. J. Baerends, F. M. Bickelhaupt, *J. Comput. Chem.* **2004**, *25*, 189.
[20] I. Vargas-Baca, M. Findlater, A. Powell, K. V. Vasudevan, A. H. Cowley, *Dalton Trans.* **2008**, 6421.
[21] This species can only be isolated as $(Ph_3P)_2Te$, and in solution exhibits a lack of coupling because of an excess of Ph_3P that cannot be avoided. T. Austad, T. Rød, K. Åse, J. Songstad, A. H. Norbury, *Acta Chem. Scand.* **1973**, *27*, 1939.
[22] C. H. W. Jones, R. D. Sharma, *Organometallics* **1987**, *6*, 1419.
[23] Y. V. Geletii, C. L. Hill, A. J. Bailey, K. I. Hardcastle, R. H. Atalla, I. A. Weinstock, *Inorg. Chem.* **2005**, *44*, 8955.
[24] The PE bond energies in Me_3PE are estimated to be 266 and 184 kJ mol^{-1} for E = Se and Te, respectively. N. Sandblom, T. Ziegler, T. Chivers, *Can. J. Chem.* **1996**, *74*, 2363.
[25] S. Hietkamp, H. Sommer, O. Stelzer, *Inorg. Synth.* **1989**, *25*, 120.
[26] For early examples of the use of phosphane tellurides R_3PTe as Te-transfer reagents, see references cited in T. Chivers, *J. Chem. Soc., Dalton Trans.* **1996**, 1185.
[27] M. L. Steigerwald, T. Siegrist, E. M. Gyorgy, B. Hessen, Y.-U. Kwon, S. M. Tanzler, *Inorg. Chem.* **1994**, *33*, 3389.
[28] A. A. Prishchenko, N. E. Nifant′ev, Z. S. Novikova, I. F. Lutsenko, *Zh. Obshch. Khim.* **1980**, *50*, 1881.
[29] P. J. W. Elder and T. Chivers, *Unpublished observations.*
[30] R. A. Zingaro, B. H. Steeves, K. Irgolic, *J. Organomet. Chem.* **1965**, *4*, 320.
[31] N. Kuhn, H. Schumann, G. Wolmerhäuser, *Z. Naturforsch. B* **1987**, *42*, 674.
[32] R. H. Blessing, *Acta Crystallogr., Sect. A* **1995**, *51*, 33.
[33] G. M. Sheldrick, *SHELX97* [Includes SHELXS97, SHELXL97, CIFTAB]. *Programs for Crystal Structure Analysis. Release 97–2*. Institüt für Anorganische Chemie der Universität, Göttingen, Germany, **1997**.
[34] G. M. Sheldrick, *Acta Crystallogr., Sect. A* **2008**, *64*, 112.
[35] G. te Velde, F. M. Bickelhaupt, E. J. Baerends, C. Fonseca Guerra, S. J. A. van Gisbergen, J. G. Snijders, T. Ziegler, *J. Comput. Chem.* **2001**, *22*, 931.
[36] C. F. Guerra, J. G. Snijders, G. te Velde, E. J. Baerends, *Theor. Chem. Acc.* **1998**, *99*, 391.
[37] E. J. Baerends, J. Autschbach, A. Bérces, C. Bo, P. M. Boerrigter, L. Cavallo, D. P. Chong, L. Deng, R. M. Dickson, D. E. Ellis, M. v. Faassen, L. Fan, T. H. Fischer, C. F. Fonseca Guerra, S. J. A. van Gisbergen, J. A. Groeneveld, O. V. Gritsenko, M. Grüning, F. E. Harris, van der P. Hoek, H. Jacobsen, G. Jensen, G. van Kessel, F. Kootstra, E. van Lenthe, D. A. McCormack, A. Michalak, V. P. Osinga, S. Patchkovskii, P. H. T. Philipsen, D. Post, C. C. Pye, W. Ravenek, P. Ros, P. R. T. Schipper, H. G. Schreckenbach, J. G. Snijders, M. Solà, M. Swart, D. Swerhone, G. te Velde, P. Vernooijs, L. Versluis, O. Visser, F. Wang, E. van Wezenbeek, G. Wiesenekker, S. K. Wolff, T. K. Woo, T. Ziegler, Amsterdam, The Netherlands http://www.scm.com ADF, Version 2010.02.
[38] S. J. A. van Gisbergen, J. G. Snijders, E. J. Baerends, *Phys. Rev. Lett.* **1997**, *78*, 3097.
[39] S. J. A. van Gisbergen, J. G. Snijders, E. J. Baerends, *J. Chem. Phys.* **1998**, *109*, 10644.
[40] S. H. Vosko, L. Wilk, M. Nusair, *Can. J. Phys.* **1980**, *58*, 1200.
[41] J. P. Perdew, *Phys. Rev. B* **1986**, *33*, 8822.
[42] J. P. Perdew, Y. Wang, *Phys. Rev. B* **1992**, *45*, 13244.
[43] E. van Lenthe, A. Ehlers, E. J. Baerends, *J. Chem. Phys.* **1999**, *110*, 8943.
[44] E. van Lenthe, E. J. Baerends, J. G. Snijders, *J. Chem. Phys.* **1993**, *99*, 4597.
[45] E. van Lenthe, E. J. Baerends, J. G. Snijders, *J. Chem. Phys.* **1994**, *101*, 9783.
[46] E. van Lenthe, J. G. Snijders, E. J. Baerends, *J. Chem. Phys.* **1996**, *105*, 6505.
[47] E. van Lenthe, R. van Leeuwen, E. J. Baerends, J. G. Snijders, *Int. J. Quantum Chem.* **1996**, *57*, 281.

Received: November 15, 2012
Published Online: April 15, 2013

